Engineering Solid Mechanics 10 (2022) 191-200

Contents lists available at GrowingScience

Engineering Solid Mechanics

homepage: www.GrowingScience.com/esm

Prediction of flow stress characteristics of P92 steel using a simple physically-based constitutive modelling

J. Obiko[a,b*], L. Chown[b,c] and D. Whitefield[b,c]

[a]*Department of Mining, Materials and Petroleum Engineering, Jomo Kenyatta University of Agriculture and Technology, Nairobi, Kenya*
[b]*School of Chemical and Metallurgical Engineering, University of the Witwatersrand,1 Jan Smuts Avenue, Johannesburg, South Africa*
[c]*DSI-NRF Centre of Excellence in Strong materials, hosted by the University of the Witwatersrand, South Africa*

ARTICLEINFO

Article history:
Received 26 January 2022
Accepted 20 April 2022
Available online
21 April 2022

Keywords:
Flow stress
Deformation
P92 steel
Material constant
Stress exponent
Uniaxial compression

ABSTRACT

This study reports the flow stress behavior of three P92 steels with different compositions. Uniaxial compression tests were conducted in the deformation temperature range of 575 °C to 650 °C and strain rate range of 0.001-0.5 s^{-1} using a Gleeble® 3500 thermo-mechanical simulator. A simple physically-based constitutive model was used to analyse the effects of deformation conditions (temperature and strain rate) on the metal flow stress behavior during the deformation process. The method accounts for the temperature dependence of Young's modulus and the lattice self-diffusion coefficient of Fe in the ferrite. Constitutive equations describing the flow stress behavior of the three P92 steels were developed. From the results, the stress exponent *n* of 26.13(steel A), 21.61(steel B) and 27.55 (steel C) were obtained using the self-diffusion activation energy in the physically-based constitutive equation. From the results, the three steels had variation in the stress exponent values, which was attributed to differences in elemental content, such as chromium and tungsten. The developed constitutive equations were verified using statistical parameters: Pearson's correlation coefficient (R) and average absolute relative errors (AARE). Statistical analysis showed that the three steels had the same R of 0.98, while AARE was: 1.68 (steel A), 1.72 (steel B), and 1.82 (steel C). The constitutive equations developed showed a good correlation between the experimental and predicted flow stress data. Hence, the method is applicable in describing flow stress behavior in the metalworking process in the industry.

1. Introduction

Characterisation of the metalworking process is complex due to the various deformation mechanisms (Lin & Chen, 2011; He et al., 2014). The flow deformation mechanisms (hardening and softening) are affected by the material response to the deformation parameters such as temperature, strain and strain rate (He et al., 2014). The deformation process for a material can be well-defined by analysing the flow stress behavior (Lin, Chen & Zhong, 2008b). Constitutive equations provide information on the effect of the deformation parameters on the flow stress behaviour. These equations can be input in computational simulation software for simulation analysis (Lin, Chen & Zhong, 2008a; Guo et al., 2009). Computer programs enhance optimisation of the process parameters, reducing trial and error and large-scale testing in the industrial production process, thus reducing the cost of optimisation and improving product quality (Zhang et al., 2009). Therefore, a well-defined constitutive equation forms an integral part of the metalworking process by increasing production efficiency (He et al., 2014). Hence, establishing accurate constitutive equations is paramount. The equations provide a mean of predicting the flow stress behaviour of commonly-used metals.

* Corresponding author.
E-mail addresses: jobiko@jkuat.ac.ke (J. Obiko)

doi: 10.5267/j.esm.2022.4.007

Constitutive models fall into two broad categories based on the computational parameters. The phenomenological models: consider continuum mechanics and thermodynamic irreversibility. The physical models: examine dislocation density theory and kinetics of dynamic recrystallisation (Lin & Chen, 2011; He et al., 2015). The phenomenological models based on regression methods are used widely because of their simplicity in the application of experiment data (Shi and Liu, 2011,Seol et al., 1999; Yang et al., 2016; Hajari et al., 2017; Luan et al., 2014). However, the physically based models (Lin et al., 2014) and neural network models (Xiao et al., 2012) have limited applications. The physical models are complex as they incorporate the material structure and the deformation micromechanism such as the dislocation movement (Haghdadi et al., 2016). The Arrhenius-type phenomenological model has wide application in predicting the flow stress behaviour of various alloys. This model has been used to analyse: modified 9Cr-1Mo steel (Samantaray, Mandal and Bhaduri, 2010), P92 steel (Shi and Liu, 2011), 35CrMo steel (Huang et al., 2017), 20CrMo alloy steel (He et al., 2013), nickel-based superalloys (Zhang et al., 2016), aluminium alloys (Lin et al., 2010), magnesium alloys (Luan et al., 2014) and titanium alloys (Jha et al., 2017). However, this model does not account for any changes occurring in the microstructure during the deformation process. Hence, the derived material constants are called apparent values (Wang et al., 2015). The activation energy calculated using the Arrhenius equation differ from the self-diffusion activation energy of iron (Fe) in austenite (270 kJ.mol^{-1}) (Cabrera, Jonas and Prado, 1996) and ferrite (239 kJ.mol^{-1}) (Ashby, 1972). This variation can be due to the microstructure changes. According to Wang *et al.* (Wang et al., 2015), the variation can be normalised by flow stress normalisation using the deformation-temperature dependent Young's Modulus *E(T)*. Therefore, the constitutive sine hyperbolic equation is as follows (Mirzadeh et al. 2011):

$$\frac{\dot{\varepsilon}}{D(T)} = B[sinh(\alpha\sigma/E(T))]^n \quad (1)$$

$$D(T) = D_0 exp\,(-Q_{sd}/RT) \quad (2)$$

$$E(T) = E_0\left[1 - \frac{T_m}{G_0}\frac{dG}{dT}\frac{(T-300)}{T_m}\right] \quad (3)$$

where D_0 is a pre-exponential constant and Q_{sd} is the self-diffusion activation energy, $E(T)$ is the value of Young's Modulus at different deformation temperatures and T_m is the melting temperature of the steel under investigation, $\dot{\varepsilon}$ is the strain rate (s^{-1}), B is the hyperbolic sine constant, α is the stress multiplier ($\alpha = B/n'$), n is the stress exponent and E_0 is the young's modulus at temperature 300K, $T_m/G_0.dG/dT$ is the temperature dependence of the modulus. G0 is the shear modulus at 300K, and D is the self-diffusion coefficient. The values of D_0, $E(T)$ and Q_{sd} are obtained from tables developed for the deformation behaviour of metals and alloys by Ashby (Ashby, 1972). The value of E_0 in Equation 3 was approximated using the equation $E_0 = 2G(1+\nu)$, in which the Poisson's ratio (ν) was taken as 0.3. There is limited literature on the application of simple physically-based constitutive modelling for predicting the flow stress behaviour of P92 steel during deformation. The study aims to investigate the possibility of utilising the physically-based constitutive model to predict the flow stress behaviour of three P92 steels during forging.

2. Experimental procedure

The slightly different chemical compositions of the three P92 steels used in this study are given in Table 1.
Round rod samples of Ø 8 mm and 12 mm length were machined from each of the three ASME P92 steel blocks. Axisymmetric compression testing was done using Gleeble® 3500 thermal-mechanical equipment under the following conditions: temperatures of 575°C to 650°C, a total strain of 0.7, and strain rates of 0.001 to 0.5 s^{-1}. The deformation temperature was controlled using K-type thermocouples welded onto the centre of the sample length. Nickel paste was applied to the graphite foil to minimise the friction effect and thermal gradient between the anvil and the specimen. The test specimens were heated up to an austenitising temperature of 1100 °C at a heating rate of 5 °C/s and held at this temperature for 180 seconds to homogenise the microstructure and reduce thermal gradients before the uniaxial compression test. The test specimens were cooled to the deformation temperature at a rate of 10 °C/s and soaked for 60 seconds, and then deformed at a specified strain rate until a strain of 0.7, and air-cooled to room temperature. The selection of the austenitisation temperature of 1100 °C was to ensure complete dissolution of $M_{23}C_6$ carbides. For these steels, carbide dissolution occurs at 850 °C according to ThermoCalc calculations, as shown in Fig. 1.

Table 1. The chemical composition of P92 steels under investigation (wt %)

Steel	C	Mn	Si	Cr	Mo	Ni	Cu	Al	V	Nb	W	Co	Fe
Steel A	0.10	0.39	0.20	8.29	0.65	0.19	0.08	0.012	0.16	0.093	2.07	0.015	Bal
Steel B	0.11	0.51	0.22	9.37	0.50	0.17	0.27	0.006	0.19	0.130	1.76	0.028	Bal
Steel C	0.11	0.32	0.25	9.48	0.61	0.17	0.00	0.023	0.20	0.076	2.34	0.024	Bal

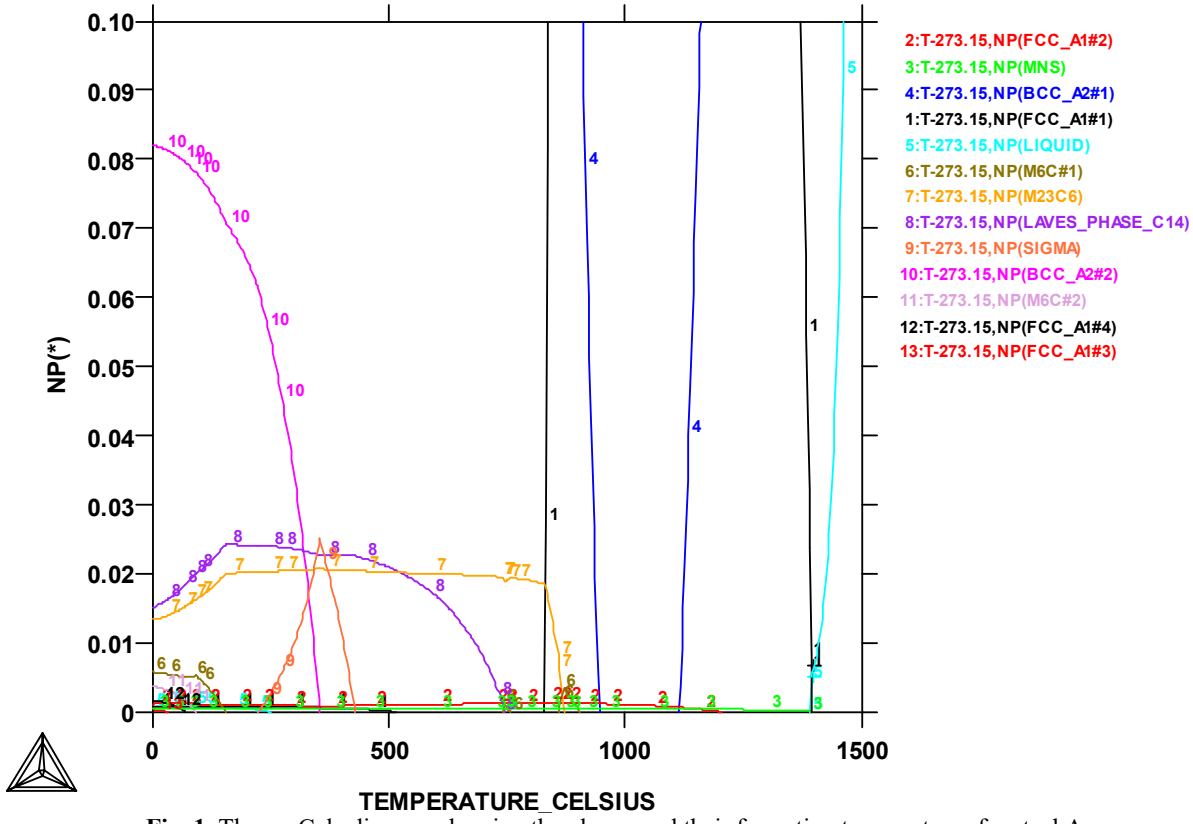

Fig. 1. ThermoCalc diagram showing the phases and their formation temperatures for steel A.

3. Results and discussion

3.1. Flow stress behaviour

3.1.1. Effect of temperature

The variation of flow stress and the deformation temperature is as given in Fig. 2 a-c) for warm deformation. The flow stress increased with a decrease in the deformation temperature and an increase in the strain rate. At a lower strain rate, the flow stress decreased with an increase in the deformation temperature. Higher temperature deformation increases the rate and extent of dynamic softening. The softening behavior is due to an increased vacancy diffusion, cross-slip and climb of edge dislocation (Xiao et al., 2012). Therefore, the dynamic softening mechanism is a thermally activated process which increases at high temperature. Metal forming is commonly done for grain refinement, hence improving material strength. However, as forming temperature increases, the average grain size increases to form equiaxed grains. The formation of equiaxed grains indicates that DRX has occurred. When 'necklace' grains (small grains occurring along the grain boundary of a large grain) occur, this implies incomplete DRX, but DRV had occurred. Metal forming at lower temperature results in a large plastic deformation force and stress, hence suitable for uniform grain refinement (Yanushkevich et al., 2016). Thus, ensure uniform fine grain distribution across the deformed sample, improving mechanical properties such as creep strength. Therefore, the effect of deformation temperature on the microstructure of the deformed sample is significant. However, forming at lower temperatures require high capacity machines. These machines result in high running costs; hence they are unpopular in the industry.

3.1.2. Effect of strain rate

Fig. 2 a-c) shows a plot of flow stress for the three P92 steels at a given strain rate. It is seen that the flow stress increases with an increase in strain rate at a given temperature. This result shows that the flow stress is sensitive to strain rate. According to Zhu et al. (2018), deformation at a higher strain rate, there is limited time for the dislocation and rearrangement to counteract, resulting in higher flow stress. However, deformation at a lower strain rate, there is sufficient time for dislocation motion and an increase of carbide precipitation, hence affecting solid solution and precipitation strength. Therefore, the flow stress variation with strain rate occur due to the deformation mechanisms which control the flow stress (Rastegari et al., 2015).

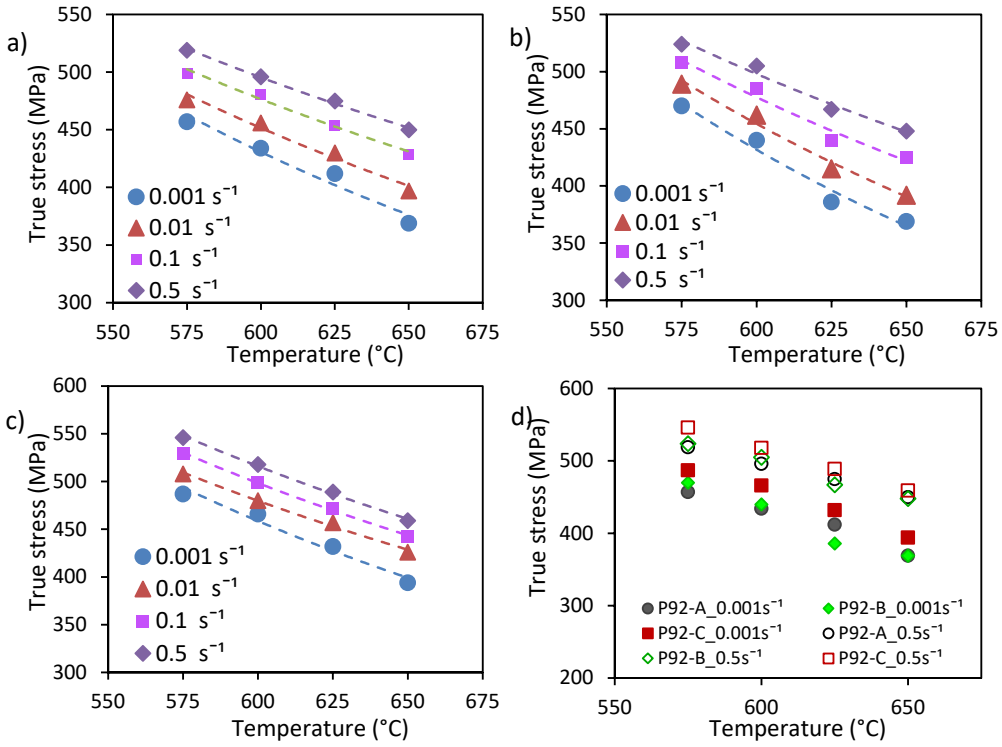

Fig. 2. The relationship between maximum flow stress, strain rate and temperature for warm deformation a) steel A, b) steel B, c) steel C and d) all the three steels

3.1.3. Effect of composition

The flow stress-strain curves of the three P92 steels showed slightly different flow stress values for all deformation conditions. Fig. 2d) shows the difference in flow stress values for the three steels tested at the lowest and the highest strain rates. Steel C had the highest flow stress in all deformation conditions. One reason may be the higher chromium content in steel C, as chromium enhances strengthening by forming precipitates that pin dislocation during deformation (Czyrska-filemonowicz et al. 2006). In this study, the test temperatures were below the dissolution temperature of $M_{23}C_6$ carbides (850 °C) for the steels investigated (Peng et al., 2017). Therefore, a high volume fraction of $M_{23}C_6$ carbides may have occurred during deformation. According to Carsi et al.(2011), a small amount of $M_{23}C_6$ carbides hinders dislocation motion, result in higher stress exponent, hence an increase in flow stress. Flow stress variation in the three steel was due to chromium content available in the steel to form carbides during deformation.

3.2. Physically-based constitutive model analysis

From Eq. (1), the only unknown material constants are B, n, and α. The saturation flow stress values (Table 2) and steel values in Table 3 were substituted in Eq. (1) and Eqs. (4-5) to determine the material constants. To determine the value of α, the power, and exponential law Eqs. (4-5) are used to determine n' and B.

$$\frac{\dot{\varepsilon}}{D(T)} = B\left(\frac{\sigma}{E(T)}\right)^{n'} \tag{4}$$

$$\frac{\dot{\varepsilon}}{D(T)} = Bexp\left(\frac{\beta'\sigma}{E(T)}\right) \tag{5}$$

From the flow stress experimental data, the plots of $ln\,\dot{\varepsilon}/D(T) - ln\,(\sigma/E(T)$ and $ln\,\dot{\varepsilon}/D(T) - (\sigma/E(T)$ were plotted and used to determine the material constant values of n' and B respectively. Then, the value of stress multiplier was calculated using the relationship of α = B/n'. According to Equation 1, the slope and the intercept of the plot of $ln\,\dot{\varepsilon}/D(T) - ln\,(sinh\,(\sigma/E(T)))$ were used to determine the value of stress exponent n and the intercept ln B respectively. The plots for determining material constants for the three steels (A, B and C) are shown in Fig. 3. The material constants for each steel have been summarised in Table 4.

Table 2. The flow stress data for the three P92 steel investigated for all the deformation conditions

Steel	Strain rate (s^{-1})	575	600	625	650
Steel A	0.001	457	434	412	369
	0.01	476	456	430	397
	0.1	499	481	454	429
	0.5	519	496	475	450
Steel B	0.001	470	440	386	369
	0.01	489	462	415	392
	0.1	508	485	440	425
	0.5	524	505	467	448
Steel C	0.001	487	466	432	394
	0.01	508	480	457	426
	0.1	529	499	472	442
	0.5	546	518	489	459

Table 3. Data for analysing the physically based model for P92 steel (Ashby, 1972)

$D_0/(m^2/s)$	Q_{sd} (KJ/mol)	η	G_0 (MPa)
2.0×10^4	251	-0.81	6.4×10^4

Table 4. The material constants of hot deformation analysis of P92 steels investigated

Steel	α	*n*	*lnB*
Steel A	344.80	26.23	38.86
Steel B	346.21	21.61	39.89
Steel C	326.90	27.55	39.53

Therefore, the resultant constitutive equation for the three steels can be written as follows:

For steel A: $$\dot{\varepsilon}\, exp\left[\frac{251000}{RT}\right] = 1.3578 \times 10^{12}[sinh(344.8 \times \sigma_{ss}/E(T))]^{26.23} \quad (6)$$

For steel B: $$\dot{\varepsilon}\, exp\left[\frac{251000}{RT}\right] = 3.7804 \times 10^{12}[sinh(346.21 \times \sigma_{ss}/E(T))]^{21.61} \quad (7)$$

For steel C: $$\dot{\varepsilon} exp\left[\frac{251000}{RT}\right] = 2.6375 \times 10^{12}[sinh(326.90 \times \sigma_{ss}/E(T))]^{27.55} \quad (8)$$

The values of material constants *α, B* and *n* were summarised as shown in Table 5. The values were obtained through linear regression fitting under different deformation conditions. Using hyperbolic sine function properties Eq. (1) can be expressed mathematically as Eq. (9):

$$\left(\frac{Z}{B}\right)^{\frac{1}{n}} = sinh\left(\alpha\frac{\sigma_{sat}}{E(T)}\right) = \frac{e^{\alpha\sigma_{sat}/E(T)}}{2} - \frac{-e^{\alpha\sigma_{sat}/E(T)}}{2} \quad (9)$$

By solving Eq. (9) this leads to Eq. (10):

$$\sigma_{sat} = \frac{E(T)}{\alpha} ln\left[\left(\frac{Z}{B}\right)^{\frac{1}{n}} + \left(\left(\frac{Z}{B}\right)^{\frac{2}{n}} + 1\right)\right]^{\frac{1}{2}} \quad (10)$$

Table 5. Calculated material constants for warm deformation

Material constants	Steel A	Steel B	Steel C
α	344.8	346.2	326.9
n	26.2	21.6	27.6
B	1.36×10^{12}	3.78×10^{12}	2.64×10^{12}

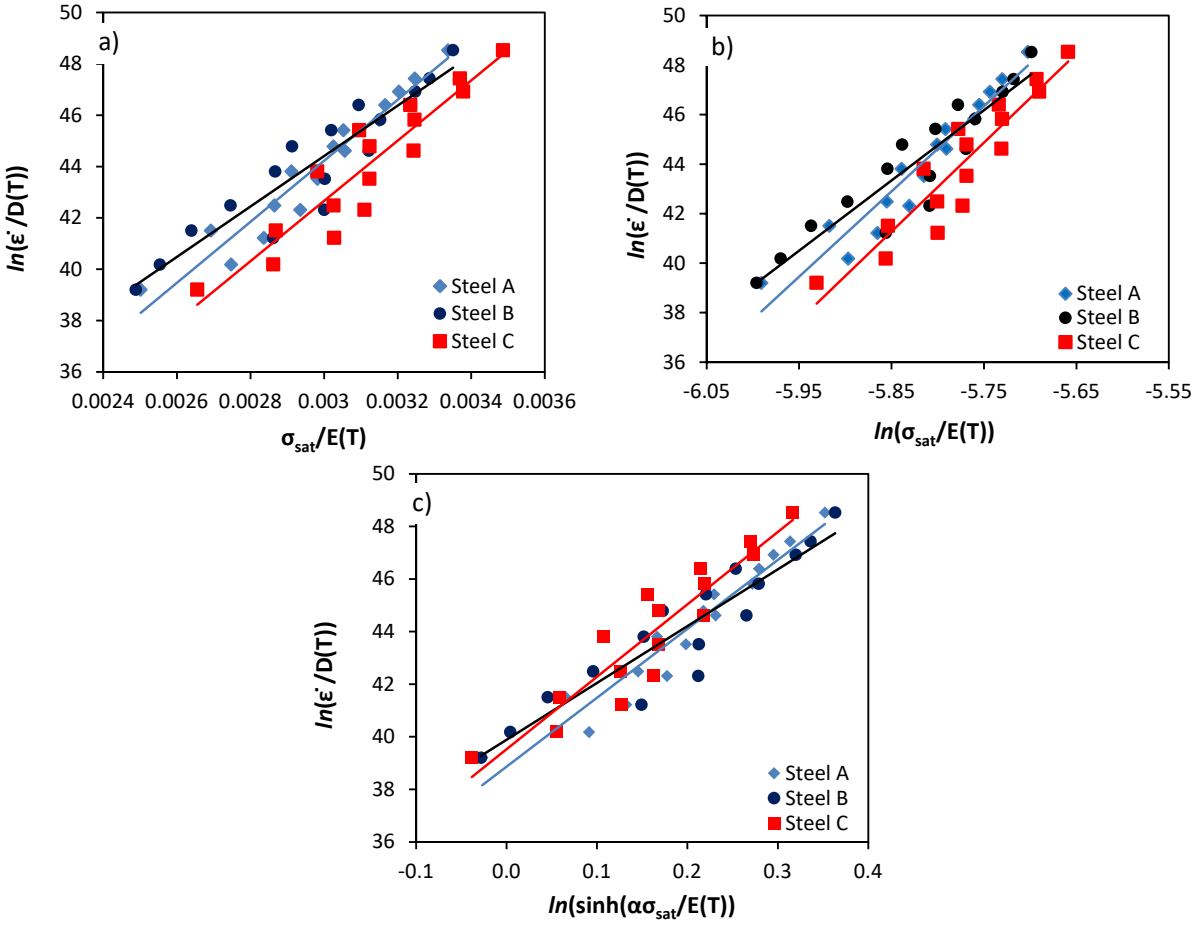

Fig. 3. The plot used to determine the material constants at saturation flow stress (a) *B* (b) *n'* (c) *n* using a simple physical based constitutive model for the three P92 steels.

From Eq. (9), the saturation flow stress under different deformation conditions can be obtained from the following equations for the three steels, and $Z = \dot{\varepsilon} exp\left(\frac{30190}{T}\right)$

For steel A: $$\sigma_{sat} = \frac{E(T)}{344.8} ln\left[\left(\frac{Z}{1.36\times10^{12}}\right)^{\frac{1}{26.2}} + \left(\left(\frac{Z}{1.36\times10^{12}}\right)^{\frac{2}{26.2}} + 1\right)\right]^{\frac{1}{2}} \quad (11)$$

For steel B: $$\sigma_{sat} = \frac{E(T)}{346.2} ln\left[\left(\frac{Z}{3.78\times10^{12}}\right)^{\frac{1}{21.6}} + \left(\left(\frac{Z}{3.78\times10^{12}}\right)^{\frac{2}{21.6}} + 1\right)\right]^{\frac{1}{2}} \quad (12)$$

For steel C: $$\sigma_{sat} = \frac{E(T)}{326.9} ln\left[\left(\frac{Z}{2.64\times10^{12}}\right)^{\frac{1}{27.6}} + \left(\left(\frac{Z}{2.64\times10^{12}}\right)^{\frac{2}{27.6}} + 1\right)\right]^{\frac{1}{2}} \quad (13)$$

3.3. Statistical error analysis of physically based model

The comparison between the predicted and experimental flow stress data for the three steels, as shown in Fig. 4. The statistical parameters: Pearson's correlation coefficient **R** (Eq. (14)) and average absolute relative error **AARE** (Eq. (15)) were employed. These parameters effectively verifies the accuracy of the developed model in predicting the flow stress of the three P92 steels (He et al., 2013; Xiao et al., 2012; Gao et al., 2014).

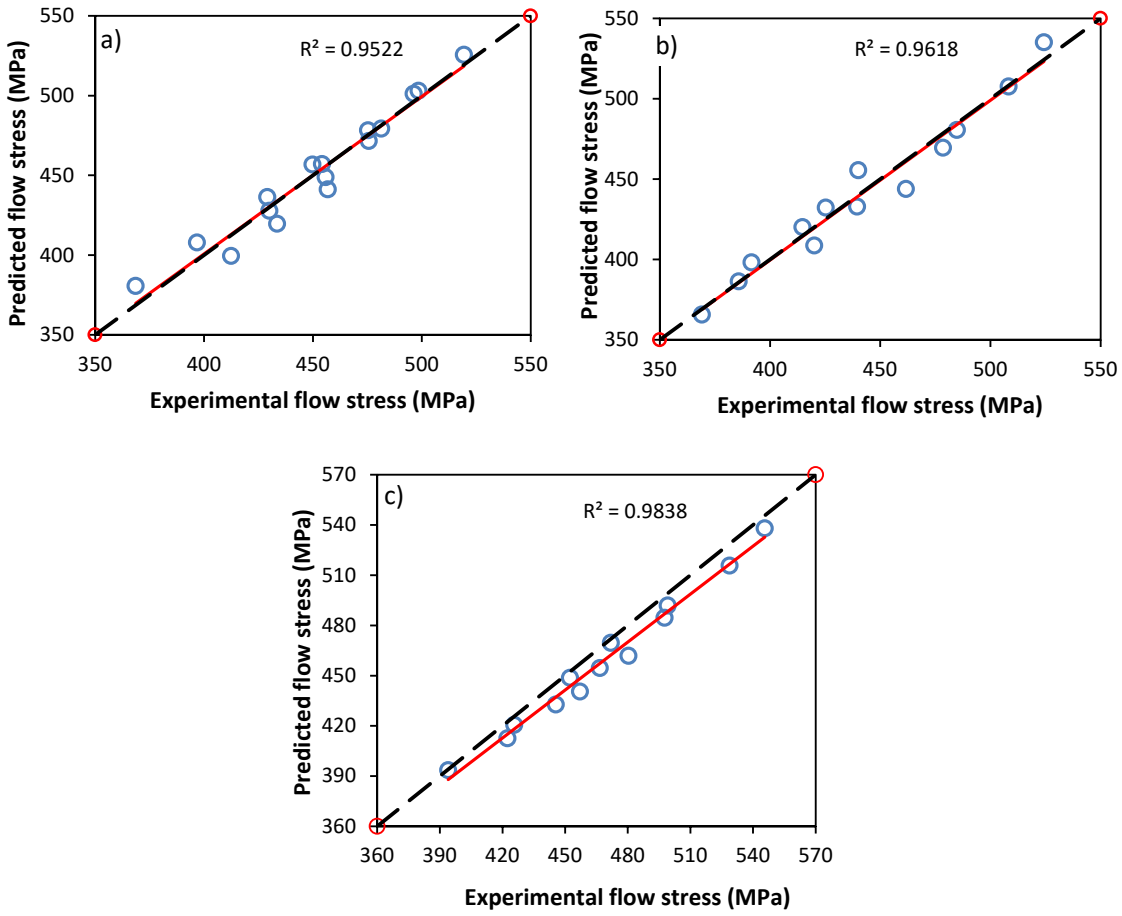

Fig. 4. Comparison between the predicted and the experimental flow stress of the three P92 steel under all the deformation conditions (a) steel A (b) steel B (c) steel C.

$$\boldsymbol{R} = \frac{\sum_{i=1}^{N}(\boldsymbol{E_i} - \bar{\boldsymbol{E}})(\boldsymbol{P_i} - \bar{\boldsymbol{P}})}{\sqrt{\sum_{i=1}^{N}(\boldsymbol{E_i} - \bar{\boldsymbol{E}})^2 \sum_{i=1}^{N}(\boldsymbol{P_i} - \bar{\boldsymbol{P}})^2}} \tag{14}$$

$$\boldsymbol{AARE}(\%) = \frac{1}{N}\sum_{i=1}^{N}\left[\frac{E_i - P_i}{E_i}\right] \tag{15}$$

where, E is the experimental flow stress, P is the predicted flow stress using the developed physically based constitutive equation and, $\bar{E}$ and $\bar{P}$ are the average values of E and P respectively. From Fig. 4, the graph shows that most of the data points lie close to the regression line showing a high coefficient of determination R^2 of 0.95 (steel A), 0.96 (steel B) and 0.98 (steel C). The calculated Pearson's correlation coefficient R for the three steels were: steel A (0.98), steel B (0.98) and steel C (0.98), while AARE values were 1.68% (steel A), 1.72% (steel B) and 1.83% (steel C). From this analysis, the results show that the developed simple physically-based constitutive model has high accuracy in predicting the flow stress behaviour for the three P92 steels investigated. Hence, this model is applicable in determining the saturation flow stress under different deformation temperatures and strain rates for P92 steels.

4. Conclusion

This study investigated the constitutive relationship of three P92 steels using a physically-based method during uniaxial compression testing at temperatures from 575 °C to 650 °C and strain rates from 0.001 s^{-1} to 0.5 s^{-1}. From the results, these were the observations:

1. During forming analysis, the self-diffusion activation energy value can be effectively and efficiently applied to the physically-based constitutive model to determine the material parameters.
2. The material constants α, n and in in the physically-based equation were determined. The results showed that this method (physically-based constitutive model) is an alternative method for predicting the flow stress during forming. The model is quick and easy to use for analysing flow stress behaviour. The physically-based model has fewer

parameters to be determined compared to the Arrhenius equation. Moreover, the model gives a physical and metallurgical background for any metal forming processes.

3. The predicted and experimental flow stress data showed a good correlation. The statistical analysis showed that the developed constitutive equations for the three steels had a high accuracy in predicting the flow stress behaviour.

Acknowledgement

The authors acknowledge and appreciates with gratitude the DST-CSIR Interbursary Support (IBS) programme for financial support.

References

Ashby, M. F. (1972). A first report on deformation-mechanism maps. *Acta Metallurgica*, *20*(7), 887–897. doi: 10.1016/0001-6160(72)90082-X.

Cabrera, J. M., Jonas, J. J., & Prado, J. M. (1996). Flow behaviour of medium carbon microalloyed steel under hot working conditions. *Materials Science and Technology*, *12*(7), 579–585. doi: 10.1179/026708396790166019.

Carsí, M., Pen˜alba, F., Rieiro, I., & Ruano A. (2011). High temperature workability behavior of a modified P92 steel', *International Journal of Materials Research*, *102*(11), 1378–1383. doi: 10.3139/146.110603.

Czyrska-filemonowicz, A., Zielińska-lipiec, A., & Ennis, P. J. (2006). Modified 9 % Cr Steels for Advanced Power Generation : Microstructure and Properties. *Journal of Achievements in Materials and Manufacturing Engineering*, *19*(2), 43–48. Available at: http://www.edu.ptnss.pb.journalamme.org/papers_vol19_2/1309.pdf.

Gao, F., Liu, Z. Misra, R., Liu, H., & Yu, F. (2014). Constitutive modeling and dynamic softening mechanism during hot deformation of an ultra-pure 17%Cr ferritic stainless steel stabilized with Nb. *Metals and Materials International*, *20*(5), 939–951. doi: 10.1007/s12540-014-5020-z.

Guo, Z., Saunders, N., Schillé, P., & Miodownik, A. P. (2009). Material properties for process simulation. *Materials Science and Engineering A*, *499*(1–2), pp. 7–13. doi: 10.1016/j.msea.2007.09.097.

Haghdadi, N., Martin, D., & Hodgson, P. (2016). Physically-based constitutive modelling of hot deformation behavior in a LDX 2101 duplex stainless steel. *Materials and Design*. Elsevier B.V., *106*, 420–427. doi: 10.1016/j.matdes.2016.05.118.

Hajari, A., Maryam, M., Abbasi, S., & Badri, H. (2017). Constitutive modeling for high-temperature flow behavior of Ti-6242S alloy. *Materials Science and Engineering A*. Elsevier, *681*(September 2016), 103–113. doi: 10.1016/j.msea.2016.11.002.

He, A., Xie, G., Zhang, H., & Wang, X. (2013). A comparative study on Johnson-Cook, modified Johnson-Cook and Arrhenius-type constitutive models to predict the high temperature flow stress in 20CrMo alloy steel. *Materials and Design*, *52*, 677–685. doi: 10.1016/j.matdes.2013.06.010.

He, A., Xie, G., Zhang, H., & Wang X. (2014). A modified Zerilli-Armstrong constitutive model to predict hot deformation behavior of 20CrMo alloy steel. *Materials and Design*, *56*, 122–127. doi: 10.1016/j.matdes.2013.10.080.

He, A., Xie, G., Yang, X., Wang, X., & Zhang, H. (2015). A physically-based constitutive model for a nitrogen alloyed ultralow carbon stainless steel. *Computational Materials Science*, *98*, 64–69. doi: 10.1016/j.commatsci.2014.10.044.

Huang Y., Wang, S., Xiao, Z., & Liu H. (2017). Critical Condition of Dynamic Recrystallization in 35CrMo Steel. *Metals*, *7*(5), 161. doi: 10.3390/met7050161.

Jha, J S., Tewari, A. M., & Sushil, T. S. (2017). Constitutive Relations for Ti-6Al-4V Hot Working. *Procedia Engineering*, *173*, 755–762. doi: 10.1016/j.proeng.2016.12.089.

Lin, Y. C., Xia, Y., Chen, X. and Chen, M. (2010). Constitutive descriptions for hot compressed 2124-T851 aluminum alloy over a wide range of temperature and strain rate. *Computational Materials Science*, *50*(1), 227–233. doi: 10.1016/j.commatsci.2010.08.003.

Lin, C., Chen, X., Wen, D., & Chen, M. (2014). A physically-based constitutive model for a typical nickel-based superalloy. *Computational Materials Science*, *83*, 282–289. doi: 10.1016/j.commatsci.2013.11.003.

Lin, Y. C., Chen, M. S., & Zhong, J. (2008a). Constitutive modeling for elevated temperature flow behavior of 42CrMo steel. *Computational Materials Science*, *42*(3), 470–477. doi: 10.1016/j.commatsci.2007.08.011.

Lin, Y. C., Chen, M. S., & Zhong, J. (2008b). Prediction of 42CrMo steel flow stress at high temperature and strain rate. *Mechanics Research Communications*, *35*(3), 142–150. doi: 10.1016/j.mechrescom.2007.10.002.

Lin, Y. C., & Chen, X. M. (2011). A critical review of experimental results and constitutive descriptions for metals and alloys in hot working. *Materials & Design*, *32*(4), 1733-1759.

Luan, J., Sun, C., Li, X., & Zhang, Q. (2014). Constitutive model for AZ31 magnesium alloy based on isothermal compression test. *Materials Science and Technology*, *30*(2), 211–219. doi: 10.1179/1743284713Y.0000000341.

Mirzadeh, H., Cabrera, J. M., & Najafizadeh, A. (2011). Constitutive relationships for hot deformation of austenite. *Acta Materialia*, *59*(16), pp. 6441–6448. doi: 10.1016/j.actamat.2011.07.008.

Peng, Y., Chen, T., Chung, T., Jeng, S., Huang, R., & Tsay, L. (2017). Creep rupture of the simulated HAZ of T92 steel compared to that of a T91 steel. *Materials*, *10*(2). doi: 10.3390/ma10020139.

Rastegari, H., Kermanpur, A., Najafizadeh, A., Porter, D., & Somani, M. (2015). Warm deformation processing maps for the plain eutectoid steels. *Journal of Alloys and Compounds*, *626*, pp. 136–144. doi: 10.1016/j.jallcom.2014.11.170.

Samantaray, D., Mandal, S., & Bhaduri, A. K. (2010). Constitutive analysis to predict high-temperature flow stress in modified

9Cr-1Mo (P91) steel. *Materials and Design*, *31*(2), pp. 981–984. doi: 10.1016/j.matdes.2009.08.012.

Seol, D., Won, Y., Yeo, T., Oh, K., Park, J., & Yim, C. (1999). High Temperature Deformation Behavior of Carbon Steel in the Austenite and Delta-Ferrite Regions. *ISIJ International*, *39*(1), pp. 91–98. doi: 10.2355/isijinternational.39.91.

Shi, R. X. and Liu, Z. D. (2011). Hot deformation behavior of P92 steel used for ultra-super-critical power plants. *Journal of Iron and Steel Research International*. *Central Iron and Steel Research Institute, 18*(7), 53–58. doi: 10.1016/S1006-706X(11)60090-3.

Wang, L., Liu, F., Cheng, J. J., Zuo, Q., & Chen, C. F. (2015). Hot deformation characteristics and processing map analysis for Nickel-based corrosion resistant alloy. *Journal of Alloys and Compounds*, *623*, 69–78. doi: 10.1016/j.jallcom.2014.10.034.

Xiao, X., Liu, G. Q., Hu, B. F., Zheng, X., Wang, L. N., Chen, S. J., & Ullah, A. (2012). A comparative study on Arrhenius-type constitutive equations and artificial neural network model to predict high-temperature deformation behaviour in 12Cr3WV steel. *Computational Materials Science*, *62*, 227–234. doi: 10.1016/j.commatsci.2012.05.053.

Yang, Z., Li, Y., Li, Y., Zhang, F., & Zhang, M. (2016). Constitutive Modeling for Flow Behavior of Medium-Carbon Bainitic Steel and Its Processing Maps. *Journal of Materials Engineering and Performance*, *25*(11), 5030–5039. doi: 10.1007/s11665-016-2301-3.

Yanushkevich, Z., Lugovskaya, A., Belyakov, A., & Kaibyshev, R. (2016). Deformation microstructures and tensile properties of an austenitic stainless steel subjected to multiple warm rolling. *Materials Science and Engineering A*. Elsevier, *667*, 279–285. doi: 10.1016/j.msea.2016.05.008.

Zhang P., Yi C., Chen G., Qin H., & Wang C. (2016). Constitutive Model Based on Dynamic Recrystallization Behavior during Thermal Deformation of a Nickel-Based Superalloy. *Metals*, 6(7), 161. doi: 10.3390/met6070161.

Zhang, Z. J., Dai, G. Z., Wu, S. N., Dong, L. X., & Liu, L. L. (2009). Simulation of 42CrMo steel billet upsetting and its defects analyses during forming process based on the software DEFORM-3D. *Materials Science and Engineering A*, 499(1–2), pp. 49–52. doi: 10.1016/j.msea.2007.11.135.

Zhu L., He J., & Zhang, Y. (2018). A two-stage constitutive model of X12CrMoWVNbN10-1-1 steel during elevated temperature. *Materials Research Express*. IOP Publishing, 5, pp. 1–11.